Thin films of fluorinated 3d-metal phthalocyanines as chemical sensors of ammonia: an optical spectroscopy study

BASOVA, Tamara V., MIKHALEVA, Natalia S., HASSAN, Aseel K <http://orcid.org/0000-0002-7891-8087> and KISELEV, Vitaly G.

Thin Films of Fluorinated *3d*-Metal Phthalocyanines as Chemical Sensors of Ammonia: an Optical Spectroscopy Study

Tamara V. Basova,*[a] Natalia S. Mikhaleva,[a] Aseel K. Hassan,[c] Vitaly G. Kiselev*[b,d]

[a]*Nikolaev Institute of Inorganic Chemistry SB RAS, 3, Lavrentieva Ave., 630090 Novosibirsk, Russia*

[b]*Novosibirsk State University, 2, Pirogova Str., 630090 Novosibirsk, Russia*

[c]*Faculty of Arts, Computing, Engineering and Sciences, Materials and Engineering Research Institute, Sheffield Hallam University, Furnival Building, 153 Arundel Street, Sheffield S1 2NU, United Kingdom*

[d]*Institute of Chemical Kinetics and Combustion SB RAS, 3, Institutskaya Str., 630090 Novosibirsk, Russia*

A comparative study of the sensor response toward gaseous ammonia of hexadecafluorinated *3d*-metal phthalocyanine ($MPcF_{16}$, M=Cu(II), Co(II), Zn(II), Ni(II)) thin films was performed using complementary experimental (viz., surface plasmon resonance, SPR, and IR absorption spectroscopy) along with theoretical (density functional theory calculations, DFT) techniques. SPR measurements revealed changes of both thickness and optical parameters (refraction indices and extinction coefficients) of the $MPcF_{16}$ films caused by adsorption of NH_3. The $MPcF_{16}$ species studied exhibited the following order of sensor response: $ZnPcF_{16}$ > $CoPcF_{16}$ ≥ $CuPcF_{16}$ > $NiPcF_{16}$. A good correlation was found between the DFT calculated (B3LYP/6-311++G(2df,p)) binding energies, experimentally measured shift of the selected IR bands, and the optical sensor response. Apart from this, we performed a detailed assignment of all intense bands in the vibrational spectra (IR and Raman) of fluorinated *3d*-metal phthalocyanines studied.

Keywords: hexadecafluorinated phthalocyanines; optical sensors; SPR; ammonia detection; vibrational spectra; DFT

1. Introduction

Ammonia (NH_3) is a toxic gas presented in large quantities in air, soil, and water. Exposure to low concentrations (25–150 ppm) of ammonia might lead to irritation of human skin, eyes, and respiratory tract. Moreover, exposure to high ammonia concentrations (> 5000 ppm) severely affects human health and can eventually lead to death [1]. Therefore, monitoring of ammonia in the gas phase is a very urgent problem in various applications, from industrial hygiene and environmental protection in chemical industry to clinical diagnostics, etc. [2] So far a huge variety of chemical sensors of ammonia have been proposed, including those based on inorganic, inorganic oxide/dioxide, and conducting polymers [3-7].

Among other materials, phthalocyanines, both unsubstituted (H_2Pc) and metal complexes (MPcs), are organic p-type semiconductors widely used as chemiresistive gas sensors. Moreover, thin films of MPcs are promising for gas sensing applications due to their high chemical and thermal stability and noticeable variations of both conductivity and optical properties upon sorption of analyte gases [8]. It is worth mentioning that both sensitivity and response of MPcs to various analytes were found to depend on the nature of the metal atom and substituents in the aromatic ring as well as on the structure and molecular organization in the thin films [8]. Therefore, the peripheral substitution of the conjugated macrocycle of MPcs by electron-withdrawing or electron-donating groups is a facile way to vary sensitivity and selectivity of their films toward different analytes [9-13]. More specifically, the electron-withdrawing fluorine peripheral substituents alter the sensitivity of MPc species toward reducing gases [10]. For instance, fluorinated zinc phthalocyanine turned out to be less sensitive to oxidizing gases (SO_2 and NO_2) and more sensitive to reducing gases (e.g., NH_3, H_2) [14, 15]. Furthermore, the same trends were observed in the electrical conductivity of ZnPc derivatives [16] in the presence of reducing gases (NH_3 and aliphatic amines), while $ZnPcF_{16}$ was noticeably more sensitive toward NH_3 and aliphatic amines than the unsubstituted ZnPc. Apart from this, the sensor response of thin films of hexadecafluorinated cobalt phthalocyanine ($CoPcF_{16}$) toward gaseous ammonia (concentration range from 50 to 1000 ppm) was also studied by total internal reflection ellipsometry [17]. Among other findings, it was demonstrated

that the specific binding of NH_3 molecules causes substantial shift of corresponding bands in the phase difference ($\Delta(\lambda)$) spectrum due to the increase in film thickness and change of its optical parameters.

Note that detailed mechanistic understanding of the sensing action of MPcs at the molecular level is crucial for further development of sensors. To this end, various optical spectroscopy techniques, both electronic (e.g., UV-vis absorption and fluorescence) and vibrational, are widely employed [18-25]. Since the vibrational spectroscopy techniques (IR and Raman) are sensitive to very tiny changes of the structure and environment at the molecular level, they are particularly useful for the study of relatively weak binding interactions between MPc substrate and chemical analytes [26-29]. The IR absorption spectroscopy can also be employed for identification of the MPc polymorphs [30-32].

On the other hand, modern quantum chemical (typically, density functional theory, DFT) calculations complement experiment in a very efficient way: viz., they provide valuable information concerning the structure of complexes of the adsorbed molecules (phthalocyanine-chemical analyte), their vibrational spectra, etc [27, 28, 33]. E.g., DFT calculations were used to calculate energies of formation and charge transfer properties of the complex of an analyte (methanol and ammonia) and ZnPc [27].

At the same time, although the vibrational spectra of metal-free phthalocyanine (H_2Pc) and a series of *3d*-metal Pcs (e.g., CuPc, ZnPc, FePc, CoPc, NiPc) were studied in detail [34-38], much less is known about vibrational spectra of their fluorinated counterparts $MPcF_{16}$. To our knowledge, Raman spectra along with vibrational reorganization energies were reported only for $CuPcF_{16}$ [39].

In the present contribution, we studied the sensor response toward ammonia vapor of hexadecafluorinated *3d*-metal phthalocyanine ($MPcF_{16}$, M=Cu(II), Co(II), Zn(II), Ni(II), Fig. 1) thin films. To this end, complementary experimental techniques (viz., surface plasmon resonance and IR absorption spectroscopy) along with theoretical calculations (DFT) were employed. Note that quantum chemical insight into the structure and energetics of the $MPcF_{16}\cdots NH_3$ complexes along with IR spectroscopy allows for deeper understanding of the sensing mechanism at the molecular level. Apart from this, we performed a detailed assignment of all intense bands in the vibrational spectra of fluorinated *3d*-metal phthalocyanines studied.

2. Experimental details

2.1. Materials

Copper and cobalt hexadecafluorophthalocyanines ($CuPcF_{16}$ and $CoPcF_{16}$) were obtained from commercial suppliers (Aldrich) and were used after purification by gradient sublimation in vacuum (10^{-5} Torr). $ZnPcF_{16}$ was synthesized in accordance with the technique described elsewhere [40]. Nickel hexadecafluorophthalocyanine ($NiPcF_{16}$) was synthesized by heating an equimolar 4:1 mixture of a sublimed 3,4,5,6-tetrafluorophthalo-1,2-dinitrile (Aldrich) and nickel acetate in a vacuum-sealed glass tube (10^{-3} Torr) for a period of 7 hours at 220 ^{o}C. The tube was afterward opened, and the mixture was washed by ethanol and acetone to remove soluble organic admixtures. All synthesized $MPcF_{16}$ species were purified by gradient sublimation in vacuum (10^{-5} Torr) at 440-450 ^{o}C.

2.2. Deposition and characterization of thin films

Thin films of $MPcF_{16}$ (M=Cu(II), Co(II), Zn(II), Ni(II)) on various substrates were obtained by organic molecular beam deposition at room temperature under vacuum conditions (10^{-5} Torr) with the deposition rate of 0.6 $nm \cdot s^{-1}$. The substrate types were varied according to particular experimental requirements for characterisation techniques employed. Namely, glass slides coated with about 40 nm thermally evaporated gold films were used as substrates for surface plasmon resonance (SPR) experiments, and (100) silicon wafers were used for vibrational spectroscopy measurements. Raman spectra were recorded with a Triplemate SPEX spectrometer equipped with CCD detector in a back-scattering geometry. The 488 nm, 100 mW line of an Ar-laser was used for excitation. Infrared spectra were recorded with a Vertex 80 FTIR spectrometer.

2.3. Quantum chemical calculations

The IR and Raman spectra of $MPcF_{16}$ and their complexes with ammonia were calculated using density functional theory (DFT) at the B3LYP/6-311++G(2df,p) [41, 42] level of theory. All calculations

were performed using Gaussian 09 suite of programs [43]. The experimental frequencies below 170 cm^{-1} were not considered because of the strong mixing of external and internal vibrations in this range. The Raman intensities were not calculated because of the resonant nature of the Raman spectra obtained using the excitation wavelength in the visible spectral range.

2.4. Evaluation of sensing properties

Surface plasmon resonance (SPR) measurements in the Kretschmann configuration were performed using $MPcF_{16}$ thin films deposited on gold coated glass substrates. The latter were brought into optical contact with a semi-cylindrical prism (refraction index n = 1.515) using an index-matching fluid. The prism/sample combination was placed on a θ-2θ rotation table driven by a microprocessor-controlled stepper motor (angular resolution 0.01°). The accuracy of the optical system corresponds to about 10^{-4}° shift of the resonance angle. Surface plasmon excitation was achieved by focusing a monochromatic *p*-polarised light beam of a He-Ne laser (λ=633 nm) onto the prism/sample interface. More detailed description of the SPR technique is given elsewhere [44, 45]. A gas cell sealed by the sample through a rubber O-ring was used to study the gaseous ammonia adsorption onto the $MPcF_{16}$ films. Kinetic SPR measurements of the intensity of reflected light at a fixed angle of incidence θ^{*}=44.2°, which was chosen to be close to the SPR minimum on the left side of the SPR curve [44], were performed in situ during exposure to NH_3 vapor of the concentration 100 and 200 ppm. In order to study the adsorption kinetics in detail the gas was diluted by mixing with air to a certain pressure and then injected into the gas cell used for the SPR measurements.

3. Results and Discussion

3.1. Surface plasmon resonance study of sensor properties of the $MPcF_{16}$ thin films

As the first step of our study, we scrutinized the sensor response of the $MPcF_{16}$ (M = Cu(II), Co(II), Zn(II), Ni(II)) thin films toward gaseous NH_3. To this end, the surface plasmon resonance (SPR) measurements were employed. Note that qualitatively similar results were obtained for all metal

phthalocyanines (MPc) studied. Fig. 2 shows the typical SPR curves representing the variation of reflected intensity as a function of internal angle of incidence for the pure gold-coated substrate (curve a, black), the thin film of as-deposited $CuPcF_{16}$ (curve b, red), and the film exposed to NH_3 gas (curve c, blue), respectively. The reflected intensity of the monochromatic p-polarised light of wavelength λ=633 nm has a minimum when the incidence angle meets a resonance condition at θ_{SPR} (Fig. 2, curve a) [46]. It seen from Fig. 2 that after deposition of $CuPcF_{16}$ film the minimum of SPR curve shifted from 44.4^o to 46.4^o (Fig. 2, curves (a) and (b)). This shift is directly related to the thickness and dielectric constant of the film [46]. The exposure of the films to ammonia vapor (200 ppm in the particular case) leads to a further shift of the SPR minimum to higher angles (Fig. 2, curve c).

The kinetic response curves upon exposure of the $MPcF_{16}$ thin films (M=Cu(II), Co(II), Zn(II), Ni(II)) to ammonia vapors of two different concentrations (100 and 200 ppm) are shown in Fig. 3. The SPR response corresponds to the intensity of reflected light detected at a fixed angle of incidence $\theta = 44.2^o$ as a function of exposure time. This particular angle of incidence was chosen to lie in a region of the SPR curve of maximum slope and close to the resonance angle for all $MPcF_{16}$ films studied (cf. Fig. 2). The time periods of exposure to lower (100 ppm) and higher (200 ppm) concentrations of NH_3, as well as of intermediate purging with fresh dry air, were chosen to be two minutes.

It is seen from Figure 3 that the response values corresponding to the steady state of adsorption were achieved in 20 seconds in all cases except $ZnPcF_{16}$ (Fig. 3(d)). The recovery times of $NiPcF_{16}$, $CoPcF_{16}$ and $CuPcF_{16}$ sensors are 15-20 seconds, while it is slightly longer (viz., 30 seconds) in the case of $ZnPcF_{16}$ film (Fig. 3(a-d)). Moreover, the sensor responses were reversible and the films were found to be stable and exhibited no significant loss in sensitivity at least after a few tens of repeated cycles of measurements. Nevertheless, further studies are necessary to determine selectivity and the detection limit of the films. Figure 3 also demonstrates that the values of photodetector response of $MPcF_{16}$ thin films depend on the nature of the central metal atom in the $MPcF_{16}$ molecule. Namely, the species studied can be arranged in the decreasing order of response: $ZnPcF_{16} > CoPcF_{16} \geq CuPcF_{16} > NiPcF_{16}$ (Fig. 3(a-d)).

In order to obtain more quantitative insight into the ammonia sensing process, we determined the changes of the film thickness *d*, refractive indices *n*, and extinction coefficients *k* (the latter are related to a complex dielectric permittivity via $\varepsilon = (n + ik)^2$) in the two cases: (a) pristine films of all $MPcF_{16}$ complexes studied and (b) those immediately after exposure to higher concentration of ammonia vapor (200 ppm). To this end, we fit the experimental SPR data by the Fresnel equations [47]. The details of a model employed are described elsewhere [48]. The results are summarized in Table 1.

Note that the adsorption of analyte molecules (NH_3 in the present case) modifies to some extent the UV-vis absorption spectra of the $MPcF_{16}$ films and, consequently, the extinction coefficient *k* at a particular wavelength [12, 49]. This, in turn, leads to increase of the refractive index, since the two values *n* and *k* are not independent and obey the Kramers-Kronig relations [50] (cf. Table 1 values). The changes of *n* and *k* upon exposure to NH_3 in the row of $MPcF_{16}$ exhibit the same trend as the above discussed response values: the most pronounced effect was observed in the case of $ZnPcF_{16}$ film (Table 1). Namely, adsorption of the gaseous ammonia results in a decrease of *n* and *k* values from 1.64 to 1.51 and from 0.26 to 0.20, respectively (Table 1). Apart from this, the increase of film thickness during NH_3 exposure (Table 1) gives evidence of film swelling.

3.2. Sensor properties at the molecular level: study of binding of ammonia to $MPcF_{16}$ films by IR spectroscopy and theoretical calculations

Among the huge variety of experimental techniques, vibrational spectroscopies (IR and Raman) have been shown to be very useful for study of the surface structure and properties of thin films [51-55]. These techniques are particularly suitable in the case of $MPcF_{16}$ compounds with unknown crystal structure, because the commonly employed X-ray diffraction methods cannot be applied directly in this case.

Note, however, that the vibrational spectroscopy methods can give insight into the structure of thin films only provided that the detailed assignment of the vibrational spectra of the deposited species is available. Unfortunately, in the particular case of fluorinated 3d-metal phthalocyanines and their

complexes with ammonia, these spectra have not been discussed in the literature. Therefore, we started from the detailed study of the vibrational spectra of $MPcF_{16}$.

3.2.1. Experimental and theoretical study of vibrational spectra of $MPcF_{16}$

The $MPcF_{16}$ complexes are planar molecules of D_{4h} point group symmetry. Assuming a D_{4h} point group for the $MPcF_{16}$ species comprised of 57 atoms, the corresponding vibrational representation reads as

$$\Gamma_{vib} = 14\,A_{1g} + 13\,A_{2g} + 14\,B_{1g} + 14\,B_{2g} + 13\,E_g + 6\,A_{1u} + 8\,A_{2u} + 7\,B_{1u} + 7\,B_{2u} + 28\,E_u.$$

The A_{1g}, B_{1g}, B_{2g}, E_g modes are Raman active, and the A_{2u} and E_u modes are IR-active. Note that A_{1g}, B_{1g}, B_{2g} are in-plane and E_g is an out-of-plane vibration. Along with experimental measurements, the vibrational spectra of all compounds under study were calculated at the B3LYP/6-311++G(2df,p) level of theory. The experimental and calculated IR and Raman spectra of $MPcF_{16}$ species studied are presented in Figs. 4 and 5, respectively. A comparison of the experimental and calculated bands in the IR and Raman spectra of $MPcF_{16}$ and their assignments are given in the Tables 2 and 3. The experimentally measured vibrational wavenumbers of $MPcF_{16}$ molecule coincide well with DFT theoretical predictions. The RMS difference between the calculated and experimental wavenumbers was 20 cm^{-1}. Note that in the case of $CuPcF_{16}$ our results are in a fairly good agreement with recent computations at a comparable level of theory [39].

It is seen from Figs. 4 and 5 that almost all vibrational modes of the same nature (both in Raman and IR spectra) have very similar wavenumbers for all four $MPcF_{16}$ species studied. However, as was pointed out earlier [38], the positions of some bands are dependent on the type of metal atom. More specifically, in the case of unsubstituted MPcs, the fundamentals lying in the spectral region between 1350 and 1500 cm^{-1} have been identified to be highly sensitive to the nature of the metal ion [36, 56]. In our case, we observed the similar features in the Raman spectra of $MPcF_{16}$, namely, the position of this band varies from 1507 cm^{-1} for $ZnPcF_{16}$ to 1549 cm^{-1} for $NiPcF_{16}$ (Table 3). The normal coordinate of this vibration is mostly comprised of displacements of the C_α-N_β-C_α bridges between the isoindole groups of the

phthalocyanine macrocycle (Tables 2 and 3) [36]. It is also worth mentioning that the variation of wavenumber of this band correlates well with the metal ion size. DFT geometry optimization yields the following values for the cavity size (more precisely, the N_α-M-N_α distance) of the metal phthalocyanines: Zn (4.00 Å) > Cu (3.94 Å) > Co (3.88 Å) > Ni (3.84 Å). These values are slightly higher (by ~ 0.05 Å) than those for the corresponding unsubstituted metal phthalocyanines [36].

Another group of fundamentals of medium intensity at 1287, 1283, 1273, and 1266 cm^{-1} for $NiPcF_{16}$, $CoPcF_{16}$, $CuPcF_{16}$, and $ZnPcF_{16}$, respectively, involves isoindole deformations (Fig. 5, Table 3). Apart from this, the fundamentals in the range 1130-1160 cm^{-1} are also sensitive to the central metal because they correspond to isoindole ring deformation coupled with C_α-N_α-C_α and C_α-N_α in-plane vibrations (Table 3). Another group of fundamentals at 937-955 cm^{-1} was attributed to the isoindole breathing along with stretching of M-N_α (Table 3). Finally, there are two groups of fundamentals in the wavenumber regions 230-280 cm^{-1} and 350-400 cm^{-1} (Fig. 5, Table 3) dominated by M-N_α in-plane and out-of-plane stretching vibrations. In addition, some bands sensitive to the nature of the metal ion are also present in the IR spectra. These fundamentals lie in the wavenumber region 1440-1530 cm^{-1} (Fig. 4, Table 2).

3.2.2. Vibrational spectra of $MPcF_{16}$ upon exposure to ammonia vapor

After detailed assignment of vibrational spectra described in the previous section, we studied the IR spectra of the films before and after exposure to ammonia (200 ppm). The frequency shifts of the selected vibrational bands in the IR spectra of all four $MPcF_{16}$ derivatives upon exposure to NH_3 are listed in Table 4. It is seen from Table 4 that the most pronounced shifts in the IR spectra were observed in the case of $ZnPcF_{16}$. The typical spectra of $ZnPcF_{16}$ before (a) and after (b) exposure to NH_3 are presented in Figure 6. Along with experimental data, the calculated vibrational frequencies of the $MPcF_{16}\cdots NH_3$ complexes are also presented in Table 4. It is worth mentioning that the NH_3 indeed forms the complex with $MPcF_{16}$ by coordination to the metal center rather than to the peripheral fluorine atoms. For instance, in the case of $ZnPcF_{16}$, the simple B3LYP estimations yielded the former complex to be ~15 kcal/mol more favourable on the enthalpy scale. This fact also agrees well with existing data on unsubstituted

MPcs [57, 58]. It is seen from Table 4 that the largest shift of IR bands of 5-6 cm^{-1} is observed in the case of $ZnPcF_{16}$. The average shift of the corresponding bands decreases to 4, 3 and 1 cm^{-1} for the $CoPcF_{16}$, $CuPcF_{16}$, and $NiPcF_{16}$ films, respectively (Table 4). The common feature of these vibrations is their sensitivity to the nature of the metal ion (Tables 2 and 3). This fact agrees well with out-of-plane distortion of the Pc core in the complex of metal phthalocyanine and ammonia (*vide infra*). Moreover, most of the discussed bands are red shifted upon exposure to NH_3, indicating that the corresponding normal coordinates become looser to some extent (Table 2). Note that the observed shifts of these particular IR bands also give evidence that the ammonia forms a complex with $MPcF_{16}$ moiety at the axial coordination position of the metal ion.

The selected DFT optimized structural parameters of $MPcF_{16}$ complexes with ammonia along with the calculated energies of complex formation are given in Table 5. It is worth mentioning that the calculated energetics of the complexes correlate well with metal-(ammonia) nitrogen bond lengths and, more importantly, with the sensor response measured by SPR technique (cf. Fig. 3, Table 1 and discussion therein). The values of relative formation enthalpies decrease in the same sequence: $ZnPcF_{16}$ > $CoPcF_{16}$ > $CuPcF_{16}$ > $NiPcF_{16}$. Note that the NH_3 axial coordination also leads to out-of-plane displacement of the central metal ion for all $MPcF_{16}$ derivatives (Table 5).

To get more insight into the interplay between microscopic structure and sensor response of the films, we compared the $MPcF_{16}\cdots NH_3$ binding energies, shifts of IR bands, and refraction index changes (Fig. 7). It is clearly seen that the energies of $MPcF_{16}\cdots NH_3$ complex formation (Table 5), red shifts of wavenumbers of some IR bonds (Table 4), and refractive index changes (Table 1) correlate well with each other (Fig. 7). Thus, on the basis of these facts we propose the variation of wavenumbers of particular IR bonds upon exposure to an analyte to be a useful descriptor for a screening among promising (i.e., those with the most pronounced changes of sensor response upon NH_3 absorption) ammonia sensors.

3.3. Comparison with similar metal phthalocyanines

Note that the sensor performance towards ammonia of several metal phthalocyanine and porphyrin species have been reported [59-61]. More specifically, the effects of the central metal atom on gas sensor performance were measured electrically (resistivity changes were monitored) for thin films of tetra-(tert-butyl)-5,10,15,20-tetraazaporphyrins ($MTAP(t\text{-}Bu)_4$, M = Pd, Ni, Co) [60], 1,8,15,22-tetra-iso-pentyloxyphthalocyanine ($MPc(iso\text{-}PeO)_4$, M = Cu, Pb, Ni) [61] and etioporphyrins (MEP) of Cu, Zn, Ni, Co, Pt, Pd [59]. It was shown that the sensor response varied in the following order: Pd > Ni > Co in the case of $MTAP(t\text{-}Bu)_4$ [60]; and Cu > Pb > Ni in the case of $MPc(iso\text{-}PeO)_4$, respectively [61]. This order has been rationalized in terms of the central ion size: the larger ion radius is, the more d-electrons participate in binding with ammonia. Note, however, that a different order of sensor response was observed in the case of MEP: CoEP > NiEP > CuEP > ZnEP [59]. It is seen that entirely different order of the sensor response was observed in the present work for strongly electron-withdrawing fluorosubstituted Pcs ($ZnPcF_{16}$ > $CoPcF_{16}$ > $CuPcF_{16}$ > $NiPcF_{16}$).

Probably, more relevant to our case are the gas sensing properties of 2,9,16,23-tetrakis(2,2,3,3-tetrafluoropropoxy) metal(II) phthalocyanines (TFPMPc, M = Co, Zn, Cu, Pb, Pd, Ni), which have also been recently scrutinized [62]. It was shown that the electrical response of TFPMPc to ammonia vapor decreases in the row Co > Zn > Cu > Pb > Pd ~Ni, which correlates well with the DFT calculated binding energies of $TFPMPc\cdots NH_3$ complexes: more specifically, the higher binding energy is, the more pronounced is the sensor response [62]. It is therefore instructive to compare these results with the findings of the present work: the sensor response order $ZnPcF_{16}$ > $CoPcF_{16}$ > $CuPcF_{16}$ > $NiPcF_{16}$ also exhibits a good correlation with the $MPcF_{16}\cdots NH_3$ binding energies (cf. Table 5 and Figure 7).

However, it should be clearly emphasized that the sensing response of a material is not solely determined by the bond strength between the central metals of the molecules of thin film and the analyte. On the contrary, many other factors can contribute noticeably: e.g., the number of active sites in a layer, tiny details of sorption-desorption process and, particularly, thickness and morphology of the film.

4. Conclusion

In the present work, adsorption of ammonia vapor to the thin films of hexadecafluorinated *3d*-metal (Cu(II), Co(II), Ni(II), Zn(II)) phthalocyanines was studied in situ using surface plasmon resonance (SPR) technique. SPR measurements revealed changes of both thickness and optical parameters (refraction indices and extinction coefficients) of the $MPcF_{16}$ films caused by adsorption of NH_3. The $MPcF_{16}$ species studied exhibited the following order of sensor response: $ZnPcF_{16}$ > $CoPcF_{16}$ ≥ $CuPcF_{16}$ > $NiPcF_{16}$. IR spectroscopy along with DFT calculations provided evidence of coordination of electron-donating NH_3 species to the metal center of $MPcF_{16}$ molecule. The most pronounced spectral shift of 5-6 cm^{-1} upon exposure to ammonia vapor was observed in case of $ZnPcF_{16}$ for the IR bands at 603, 654, 937, 960, 1148 and 1266 cm^{-1}. These shifts are mainly due to axial coordination of NH_3 to the metal ion leading to out-of-plane distortion of the MPc core. A good correlation was found between the DFT calculated binding energies, experimentally measured shift of the selected IR bands and the optical sensor response.

Acknowledgements

The funding by the Russian Science Foundation (project # 15-13-10014) is gratefully acknowledged.

References

[1] J. E. Ryer-Powder, Health effects of ammonia, Plant/Operations Prog., 10 (1991) 228–232 and refs therein.

[2] B. Timmer, W. Olthuis, A. Van den Berg, Ammonia sensors and their applications - a review, Sens. Actuat. B: Chem. 107 (2005) 666–677.

[3] E.C. Dickey, O.K. Varghese, K.G. Ong, D. Gong, M. Paulose, C. Grimes, C.A. Grimes, Room temperature ammonia and humidity sensing using highly ordered nanoporous alumina films, Sensors 2 (2002) 91–110.

[4] J. Huang, J. Wang, C. Gu, K. Yu, F. Meng, J. Liu, A novel highly sensitive gas ionization sensor for ammonia detection, Sens. Actuat. A: Phys. 150 (2009) 218–223.

[5] S. Koul, R. Chandra, S. Dhawan, Conducting polyaniline composite: a reusable sensor material for aqueous ammonia, Sens. Actuat. B: Chem. 75 (2001) 151–159.

[6] H. Tai, Y. Jiang, G. Xie, J. Yu, X. Chen, Fabrication and gas sensitivity of polyaniline-titanium dioxide nanocomposite thin film, Sens. Actuat. B: Chem. 125 (2007) 644–650.

[7] L. Torsi, M. Pezzuto, P. Siciliano, R. Rella, L. Sabbatini, L. Valli, P.G. Zambonin, Conducting polymers doped with metallic inclusions: New materials for gas sensors, Sensors Actuators B, 48 (1998) 362–367.

[8] A.W. Snow, W.R. Barger, Phthalocyanine Films in Chemical Sensors, in: C.C. Leznoff, A.B.P. Lever (Eds.), Phthalocyanine properties and applications, V.1, Weinheim, Germany: VCH, 1989, p. 341–392.

[9] T. Miyata, S. Kawaguchi, M. Ishii, T. Minami, High sensitivity chlorine gas sensors using Cu-phthalocyanine thin films, Thin Solid Films 425 (2003) 255–259.

[10] F.I. Bohrer, C.N. Colesniuc, J. Park, I.K. Schuller, A.C. Kummel, W.C. Trogler, Selective detection of vapor phase hydrogen peroxide with phthalocyanine chemiresistors, J. Am. Chem. Soc. 130 (2008) 3712–3713.

[11] J. Spadavecchia, G. Ciccarella, R. Rella, S. Capone, P. Siciliano, Variation in the optical sensing responses toward vapors of a porphyrin/phthalocyanine hybrid thin film, Chem. Mat. 16 (2004) 2083–2090.

[12] J. Spadavecchia, G. Ciccarella, R. Rella, S. Capone, P. Siciliano, Metallophthalocyanines thin films in array configuration for electronic optical nose applications, Sens. Actuators B: Chem. 96 (2003) 489–497.

[13] L. Valli, Phthalocyanine-based Langmuir–Blodgett films as chemical sensors, Adv. Col. Interface Sci. 116 (2005) 13–44.

[14] B. Schollhorn, J.P. Germain, A. Pauly, C. Maleysson, J.P. Blanc, Influence of peripheral electron-withdrawing substituents on the conductivity of zinc phthalocyanine in the presence of gases. Part 1: reducing gases, Thin Solid Films 326 (1998) 245–250.

[15] J.P. Germain, A. Pauly, C. Maleysson, J.P. Blanc, B. Schöllhorn, Influence of peripheral electron-withdrawing substituents on the conductivity of zinc phthalocyanine in the presence of gases. Part 2: oxidizing gases, Thin Solid Films 333 (1998) 235–239.

[16] X. Ma, H. Chen, M. Shi, G. Wu, M. Wang, J. Huang, High gas-sensitivity and selectivity of fluorinated zinc phthalocyanine film to some non-oxidizing gases at room temperature, Thin Solid Films 489 (2005) 257–261.

[17] T. Basova, A. Hassan, Ammonia sorption studies into thin layers of hexadecafluorinated cobalt phthalocyanine using optical techniques, J. Porphyrins Phthalocyanines 17 (2013) 934–940.

[18] J. Spadavecchia, R. Rella, P. Siciliano, M.G. Manera, A. Alimelli, R. Paolesse, C. Di Natale, A. D'Amico, Optochemical vapour detection using spin coated thin film of ZnTPP, Sens. Actuat. B: Chem. 115 (2006) 12–16.

[19] Q. Yan, J. Yuan, Y. Kang, Z. Cai, L. Zhou, Y. Yin, Dual-sensing porphyrin-containing copolymer nanosensor as full-spectrum colorimeter and ultra-sensitive thermometer, Chem. Commun. 46 (2010) 2781–2783.

[20] M.B. Winter, E.J. McLaurin, S.Y. Reece, C. Olea Jr., D.G. Nocera, M.A. Marletta, Ru-Porphyrin Protein Scaffolds for Sensing O-2, J. Am. Chem. Soc. 132 (2010) 5582–5583.

[21] R. Selyanchyn, S. Korposh, W. Yasukochi, S.-W. Lee, Optical fibre long period grating with a nanoporous coating formed from silica nanoparticles for ammonia sensing in water, Sens. Transduc. 125 (2011) 54–67.

[22] S.A. Brittle, T.H. Richardson, A.D.F. Dunbar, S.M. Turega, C.A. Hunter, Tuning free base tetraphenylporphyrins as optical sensing elements for volatile organic analytes, J. Mater. Chem. 21 (2011) 4882–4887.

[23] Y. Itagaki, S. Yamanaka, Y. Sadaoka, HCl Detection Using Polymer-Porphyrin Composite Coated Optical Fiber Sensor, Sens. Lett. 9 (2011) 114–117.

[24] H. Supriyatno, K. Nakagawa, Y. Sadaoka, Optochemical sensor for HCl gas based on tetraalkoxyphenylporphyrin dispersed in an acrylate polymer matrix, Sens. Mater. 13 (2001) 359–371.

[25] R. Rella, A. Rizzo, A. Licciulli, P. Siciliano, L. Troisi, L. Valli, Tests in controlled atmosphere on new optical gas sensing layers based on TiO_2/metal-phthalocyanines hybrid system, Mater. Sci. Eng. C 22 (2002) 439–443.

[26] T.V. Basova, E.K. Kol'tsov, I.K. Igumenov, Spectral investigation of interaction of copper phthalocyanine with nitrogen dioxide, Sens. Actuat. B: Chem. 105 (2005) 259–265.

[27] G.S.S. Saini, S. Singh, S. Kaur, R. Kumar, V. Sathe, S.K. Tripathi, Zinc phthalocyanine thin film and chemical analyte interaction studies by density functional theory and vibrational techniques, J. Phys.: Condens. Matter. 21 (2009) 225006.

[28] G.S.S. Saini, S.D. Dogra, K. Sharma, S. Singh, S.K. Tripathi, V. Sathe, R.K. Singh, Experimental and density functional theoretical study of the effects of chemical vapours on the vibrational spectra of nickel phthalocyanine thin films, Vib. Spectrosc. 57 (2011) 61–71.

[29] L. Giotta G. Giancane, D. Mastrogiacomo, T. Basova, P. Metrangolo, L. Valli, Phenol chemisorption onto phthalocyanine thin layers probed by ATR-FTIR difference spectroscopy, Phys. Chem. Chem. Phys. 11 (2009) 2161–2165.

[30] G. Maggioni, A. Quaranta, S. Carturan, A. Patelli, M. Tonezzer, R. Ceccato, G.D. Mea, Deposition of copper phthalocyanine films by glow-discharge-induced sublimation, Chem. Mater. 17 (2005) 1895–1904.

[31] M.M. El-Nahass, K.F. Abd-El-Rahman, A.A.A. Darwish, Fourier-transform infrared and UV-vis spectroscopes of nickel phthalocyanine thin films, Mater. Chem. Phys. 92 (2005) 185–189.

[32] T.V. Basova, V.G. Kiselev, I.S. Dubkov, S.A. Gromilov, F. Latteyer, H. Peisert, T. Chassè, Optical Spectroscopy and XRD Study of Molecular Orientation, Polymorphism, and Phase Transitions in Fluorinated Vanadyl Phthalocyanine Thin Films, J. Phys. Chem. C 117 (2013) 7097–7106.

[33] M.-S. Liao, S. Scheiner, Electronic structure and bonding in metal phthalocyanines, Metal=Fe, Co, Ni, Cu, Zn, Mg, J. Chem. Phys. 114 (2001) 9780–9791.

[34] S. M. Bayliss, S. Heutz, G. Rumbles, T. S. Jones, Thin film properties and surface morphology of metal free phthalocyanine films grown by organic molecular beam deposition, Phys. Chem. Chem. Phys. 1 (1999) 3673–3676.

[35] D.R. Tackley, G. Dent, W.E. Smith, IR and Raman assignments for zinc phthalocyanine from DFT calculations, Phys. Chem. Chem. Phys. 2 (2000) 3949–3955.

[36] D.R. Tackley, G. Dent, W.E. Smith, Phthalocyanines: structure and vibrations, Phys. Chem. Chem. Phys. 3 (2001) 1419–1426.

[37] D. Li, Z. Peng, L. Deng, Y. Shen, Y. Zhou, Theoretical studies on molecular structure and vibrational spectra of copper phthalocyanine, Vib. Spectrosc. 39 (2005) 191–199.

[38] T.V. Basova, V.G. Kiselev, B. Schuster, H. Peisert, T. Chasse, Experimental and theoretical investigation of vibrational spectra of copper phthalocyanine: polarized single-crystal Raman spectra, isotope effect and DFT calculations, J. Raman Spectr. 40 (2009) 2080–2087.

[39] F-C. Wu, H.-L. Cheng, C.-H. Yen, J.-W. Lin, S.-J. Liu, W.-Y. Chou, F.-C. Tang, Electron transport properties in fluorinated copper-phthalocyanine films: importance of vibrational reorganization energy and molecular microstructure, Phys. Chem. Chem. Phys. 12 (2010) 2098–2106.

[40] P. Semyannikov, T. Basova, S. Trubin, E. Kol'tsov, I. Igumenov, Vapor pressure measurements and thermodynamics of some volatile phthalocyanines, J. Porph. Phthalocyanines 10 (2006) 1034–1039.

[41] A.D. Becke, Density-functional thermochemistry. 3. The role of exact exchange, J. Chem. Phys. 98 (1993) 5648–5652.

[42] C. Lee, W. Yang, R.G. Parr, Development of the Colle-Salvetti correlation - energy formula into a functional of the electron density, Phys. Rev. B 37 (1988) 785–789.

[43] M.J. Frisch, G.W. Trucks, H.B. Schlegel, G.E. Scuseria, M.A. Robb, J.R. Cheeseman, G. Scalmani, V. Barone, B. Mennucci, G.A. Petersson et al., Gaussian 09, Revision A.01; Gaussian:Wallingford, CT, USA, 2004.

[44] A.V. Nabok, A.K. Hassan, A.K. Ray, O. Omar, V.I. Kalchenko, Study of adsorption of some organic molecules in calix[4]resorcinolarene LB films by surface plasmon resonance, Sens. Actuat. B: Chem. 45 (1997) 115–121.

[45] A.V. Nabok, A. Tsargorodskaya, A.K. Hassan, N.F. Starodub, Total internal reflection ellipsometry and SPR detection of low molecular weight environmental toxins, Appl. Surf. Sci. 246 (2005) 381–386.

[46] P. Englebienne, A.V. Hoonacker, M. Verhas, Surface plasmon resonance: principles, methods and applications in biomedical sciences, Spectroscopy 17 (2003) 255–273 and refs therein.

[47] I. Pockrand, Surface plasma oscillations at silver surfaces with thin transparent and absorbing coatings, Surf. Sci. 72 (1978) 577–588.

[48] A. Nabok, A. Tsargorodskaya, The method of total internal reflection ellipsometry for thin film characterisation and sensing, Thin Solid Films 516 (2008) 8993–9001.

[49] J. Spadavecchia, G. Ciccarella, R. Rella, Optical characterization and analysis of the gas/surface adsorption phenomena on phthalocyanines thin films for gas sensing application, Sens. Actuat. B: Chem. 106 (2005) 212–220.

[50] V. Lucarini, J.J. Saarinen, K.-E. Peiponen, E.M. Vartiainen, Kramers-Kronig Relations in Optical Materials Research, in: Springer Series in Optical Sciences, V.110, Springer, 2005.

[51] R. Aroca, A. Thedchanamoorthy, Vibrational studies of molecular organization in evaporated phthalocyanine thin solid films, Chem. Mater. 7 (1995) 69−74.

[52] T. Del Cano, V. Parra, M.L. Rodrıguez-Mendez, R.F. Aroca, J.A. De Saja, Characterization of evaporated trivalent and tetravalent phthalocyanines thin films: Different degree of organization, Appl. Surf. Sci. 246 (2005) 327−333.

[53] C.A. Jennings, R. Aroca, G.J. Kovacs, C. Hsaio, FT-Raman spectroscopy of thin films of titanyl phthalocyanine and vanadyl phthalocyanine, J. Raman Spectrosc. 27 (1996) 867−872.

[54] T.V. Basova, V.G. Kiselev, L.A. Sheludyakova, I.V. Yushina, Molecular organization in the thin films of chloroaluminium hexadecafluorophthalocyanine revealed by polarized Raman spectroscopy, Thin Solid Films 548 (2013) 650–656.

[55] T.V. Basova, V.G. Kiselev, F. Latteyer, H. Peisert, T. Chassé, Molecular organization in the thin films of gallium(III) phthalocyanine chloride and its mu-(oxo) dimer: Optical spectroscopy and XPS study, Appl. Surf. Sci. 322 (2014) 242–248.

[56] G. Dent, F. Farrell, NIR FT Raman examination of phthalocyanines at 1064 nm, Spectrochim. Acta A 53 (1997) 21–23.

[57] F.I. Bohrer, C.N. Colesniuc, J. Park, M.E. Ruidiaz, I.K. Schuller, A.C. Kummel, W.C. Trogler, Comparative Gas Sensing in Cobalt, Nickel, Copper, Zinc, and Metal-Free Phthalocyanine Chemiresistors, J. Am. Chem. Soc. 131 (2009) 478–485.

[58] F.I. Bohrer, A. Sharoni, C. Colesniuc, J. Park, I.K. Schuller, A.C. Kummel, W.C. Trogler, Gas sensing mechanism in chemiresistive cobalt and metal-free phthalocyanine thin films, J. Am. Chem. Soc. 129 (2007) 5640–5646.

[59] M.A. Goldshtrakh, N.N. Kononov, S.G. Dorofeev, A.A. Ischenko, Gas sensitivity of etioporphyrin metal complexes in thin films, J. Anal. Chem. 64 (2009) 1247–1251.

[60] B. Wang, Z. Chen, X. Zuo, Y. Wu, C. He, X. Wang, Z. Li, Comparative NH3-sensing in palladium, nickle and cobalt tetra-(tert-butyl)-5,10,15,20-tetraazaporphyrin spin-coating films, Sens. Actuators B: Chem. 160 (2011) 1–6.

[61] B. Wang, X. Zhou, Y. Wu, Z. Chen, C. He, X. Zu, Preparation, characterization and NH3-sensing of 1,8,15,22-tetra-iso-pentyloxyphthalocyanine copper, nickel and lead spin-coating films, Sens. Actuators B: Chem. 161 (2012) 498–503.

[62] X. Liang,; Z. Chen, H. Wu, L. Guo, C. He, B. Wang, Y. Wu, Enhanced NH_3-sensing behavior of 2,9,16,23-tetrakis(2,2,3,3-tetrafluoropropoxy) metal(II) phthalocyanine/multi-walled carbon nanotube hybrids: An investigation of the effects of central metals, Carbon 80 (2014) 268–278.

Table 1. Thickness (*d*), Indices of Refraction (*n*), and Extinction Coefficients (*k*) for Pristine and NH_3 Exposed $MPcF_{16}$ Films (200 ppm).

	Pristine films			NH_3 exposed films		
	n (λ=633 nm)	*k* (λ=633 nm)	*d*, nm	Δ*n*/*n*, %	Δ*k*/*k*, %	Δ*d*/*d*, %
$ZnPcF_{16}$	1.64	0.26	34	7.9	23	18
$CoPcF_{16}$	1.52	0.20	22	6.1	19	16
$CuPcF_{16}$	1.49	0.22	27	5.2	13	11
$NiPcF_{16}$	1.59	0.28	30	2.5	4	4

Table 2. Experimental and Calculated (B3LYP/6-311++G(2df,p)) IR Wavenumbers (cm^{-1}) of $MPcF_{16}$. The Atomic Labels Are in Accordance with Fig. 1.

$ZnPcF_{16}$		$CoPcF_{16}$		$CuPcF_{16}$		$NiPcF_{16}$		Sym-metry	Assignments
Expt	Calcd.	Expt	Calcd.	Expt	Calcd.	Expt	Calcd.		
196	198	227	205	228	203	229	207	E_u	C_α-C_β-C_γ, N_α-M-N_α IP
229	220	275	268	252	245	280	272	A_{2u}	M-N_α OOP, F out-of-plane motions
262	277	314	280	280	279	320	282	E_u	C_δ-C_δ-F, C_γ-C_δ-F IP
281	284		296		288		298	E_u	C_δ-C_δ-F, C_δ-C_γ-F IP
293	325		338	313	329		339	E_u	M-N_α, C_β-C_γ-F, C_γ-C_δ-F
329	329	341	366	337	340		374	A_{2u}	N_α and N_β OOP motions, M-N_α
352	372	367	407	350	381	369	411	E_u	M-N_α, N_β-C_α-C_β, C_α-C_β-C_γ
370	390	389	388	381	387	392	392	A_{2u}	N_β out-of-plane motions, C_α-C_β-C_γ OOP, isoindole OOP deformations
428	461	428	462	428	462	428	465	E_u	C_β-C_γ-C_δ, M-N_α
496	497	499	499	497	498	498	502	E_u	benzene def., N_β-C_α-C_β
603	603	605	605	603	603	606	606	E_u	macroring breathing, M-N_α
654	658	663	663	657	659	674	667	E_u	C_α-N_α-C_α, M-N_α, C_β-C_β-C_γ, C_α-C_β-C_γ
746	764	754	769	749	768	754	774	E_u	C_α-N_β-C_α, C_α-C_β-C_β, C_β-C_γ-F, C_γ-C_γ-F, C_γ-C_δ-F IP
766	782	769	788	768	784	770	792	A_{2u}	C_α and N_α out-of-plane motions
835	836	844	846	839	843	846	852	E_u	C_β-C_α-N_β, C_β-C_β-C_γ, C_α-N_β-C_α IP
937	937	953	952	947	944	955	957	E_u	C-F, isoindole breathing, C_α-N_β-C_α, C_α-C_β, M-N_α IP
960	963	966	969	963	967	968	976	E_u	Macroring breathing, C-F, M-N_α IP
1072	1074	1075	1080	1073	1077	1076	1086	E_u	C_α-N_α, C_α-N_α-C_α, C_β-C_β-C_γ IP
1130	1142	1142	1145	1141	1145	1142	1150	E_u	Benzene def., C-F, C_α-N_α-C_α, C_α-N_α IP
1148	1150	1157	1156	1152	1154	1158	1162	E_u	Benzene def., C-F, C_α-N_α-C_α, C_α-N_α IP
1266	1268	1283	1285	1273	1278	1287	1292	E_u	isoindole def., C_α-N_β, C_β-C_β IP
1312	1311	1325	1325	1320	1321	1328	1329	E_u	C_β-C_β, C_β-C_γ, C_γ-C_δ, benzene def. IP
1334	1327	1350	1334	1337	1334	1356	1332	E_u	Pyrrole def., C_α-N_α, C_α-C_β IP
	1343		1347		1345	1407	1357	E_u	macroring def.
1449	1451	1469	1468	1460	1462	1472	1477	E_u	C_α-N_β, C_α-C_β, C_δ-C_δ, C_β-C_α-N_α IP
1479	1483	1497	1500	1489	1490	1500	1512	E_u	C_α-N_β, C_β-C_β, C_δ-C_δ, C_γ-C_δ IP
1490	1495	1505	1516	1507	1512	1508	1526	E_u	C_α-N_β, C_γ-C_δ, C_α-N_α IP
1613	1611	1529	1531	1526	1521	1533	1547	E_u	C_β-C_γ, C_γ-C_δ, C_α-N_β
1639	1639	1622	1618	1617	1617	1625	1627	E_u	C_β-C_β, C_δ-C_δ
1639	1639	1639	1639	1636	1636	1640	1640	E_u	C_β-C_γ, C_γ-C_δ

Table 3. Experimental and Calculated (B3LYP/6-311++G(2df,p)) Raman Shifts (cm^{-1}) of $MPcF_{16}$. The Atomic Labels Are in Accordance with Fig. 1.

$ZnPcF_{16}$		$CoPcF_{16}$		$CuPcF_{16}$		$NiPcF_{16}$		Sym-metry	Assignments
Expt	Calcd	Expt	Calcd	Expt	Calcd	Expt	Calcd		
120	116	144	139	127	126	133	138	B_{1g}	M-N_α, macrocycle breath.
176	172	174	173	175	173	174	174	A_{1g}	macrocycle breath.
201	198	205	205	203	200	208	207	B_{2g}	N_α-M-N_α, C_α-N_β-C_α IP
279	279	281	282	279	280	281	283	B_{2g}	C_β-C_γ-F, C_γ-C_δ-F, N_α-M-N_α
322	316	326	320	322	317		322	B_{1g}	C_β-C_γ-F, M-N_α
332	320	332	326	332	323	331	329	B_{2g}	N_α-M-N_α, C_β-C_γ-F, M-N_α
369	330	368	330	368	331		332	A_{1g}	C_β-C_γ-F, macrocycle breath., M-N_α
426	437	421	444	424	440		447	B_{1g}	C_β-C_γ-C_δ, M-N_α, macrocycle breath. asym.
468	465	466	466	467	467	469	469	A_{1g}	C_β-C_γ-C_δ, M-N_α, macrocycle breath. sym.
512	513	509	514	510	514	511	516	B_{2g}	benzene def.
554	555	553	569	559	560	556	571	B_{1g}	M-N_α, macrocycle breath.
585	583	584	585	583	583	585	587	A_{1g}	M-N_α, inner ring breath., C_α-N_α-C_α
728	724	734	733	733	729	739	739	A_{1g}	C_α-N_β-C_α, N_α-C_α-N_β, M-N_α
743	753	747	756	746	751	752	758	B_{1g}	N_β-C_α-N_β, inner ring def., M-N_α IP
768	773	767	772	768	773	770	777	B_{2g}	C_α-N_β-C_α, C_α-C_β-C_β, C_β-C_γ-F, C_γ-C_γ-F IP
811	813	815	819	814	817	819	825	B_{2g}	C_β-C_α-N_β, C_β-C_β-C_γ, C_α-N_β-C_α IP
946	959	967	962	964	961	965	967	A_{1g}	Macroring breathing, C-F IP
1059	1067	1062	1070	1065	1069	1069	1077	B_{2g}	C_α-N_α, N_α-M-N_α, isoindole def. IP
1135	1139	1133	1142	1135	1142	1112	1137	A_{1g}	Benzene def., C-F, C_α-N_α-C_α IP
1193	1196	1189	1196	1193	1197	1193	1201	B_{2g}	C_α-N_α, isoindole def., C_δ-F IP
1303	1295	1312	1307	1308	1303	1303	1313	B_{1g}	C_α-N_α-C_α, C_α-C_β-C_β
	1297		1316		1309		1328	A_{1g}	C_β-C_β, C_γ-F IP
	1308		1314		1312		1322	B_{2g}	C_α-N_α, benzene def. IP
	1310		1328		1322		1341	B_{1g}	C_β-C_β, C_δ- C_δ, benzene def. IP
1342	1346	1331	1342	1339	1345	1335	1349	A_{1g}	macroring def.
1354	1355	1363	1362	1360	1359	1377	1372	B_{1g}	C_α-C_β, C_β-C_γ, benzene def. IP
1399	1398	1396	1405	1404	1404	1411	1416	A_{1g}	macroring def.
1441	1472	1479	1480	1460	1480	1488	1490	A_{1g}	Benzene breathing, C_α-N_β
1474	1479	1492	1481	1483	1481	1505	1489	B_{1g}	C_β-C_β, C_δ-C_δ, C_β-C_γ, C_α-N_β
1507	1511	1524	1541	1522	1528	1549	1560	A_{1g}	C_α-N_β, C_α-C_β
1536	1550	1536	1580	1536	1567	1560	1595	B_{1g}	C_α-N_β
1612	1614	1615	1620	1616	1620	1623	1630	A_{1g}	C_β-C_β, C_δ-C_δ, C_γ-C_δ
1630	1630	1633	1633	1633	1633	1637	1637	B_{2g}	C_β-C_γ, C_γ-C_δ

Table 4. Experimental Wavenumbers (cm^{-1}) of the Selected IR Bands of $MPcF_{16}$ Thin Films Before and After Exposure to Ammonia Vapor and DFT Calculated (B3LYP/6-311++G(2df,p)) Wavenumbers of the Axially Coordinated $MPcF_{16}\cdots NH_3$ Complexes.

$ZnPcF_{16}$				$CoPcF_{16}$				$CuPcF_{16}$				$NiPcF_{16}$			
expt		calcd		expt		calcd		expt		calcd		expt		calcd	
Pristine film	NH_3 expos.	$MPcF_{16}$	$MPcF_{16}\cdots NH_3$	Pristine film	NH_3 expos.	$MPcF_{16}$	$MPcF_{16}\cdots NH_3$	Pristine film	NH_3 expos.	$MPcF_{16}$	$MPcF_{16}\cdots NH_3$	Pristine film	NH_3 expos.	$MPcF_{16}$	$MPcF_{16}\cdots NH_3$
603	597	603	597	605	603	605	602	603	601	603	600	606	606	606	605
654	648	658	653	663	658	663	661	657	655	659	657	674	674	667	667
937	**926**	**937**	**931**	**953**	**948**	**952**	**948**	**947**	**945**	**944**	**941**	**955**	**954**	**957**	**956**
960	956	963	957	966	962	969	966	963	960	967	964	968	967	976	975
1148	1142	1150	1144	1158	1154	1156	1153	1152	1149	1154	1151	1158	1158	1162	1161
1266	1261	1268	1264	1283	1278	1285	1281	1273	1272	1278	1275	1287	1287	1292	1291

Table 5. The M-NH_3 (M=Co, Cu, Ni, Zn) Bond Lengths (in Å), N_α-M-N_α Angles (degrees), Relative Electronic Energies (ΔE), Enthalpies ($\Delta(\Delta H^0)$), and Gibbs Free Energies ($\Delta(\Delta G^0)$) of Complex Formation (at 298 K in the Gas Phase) of the Various $MPcF_{16}\cdots NH_3$ Compounds Calculated at the B3LYP/6-311++G(2df,p) Level of Theory.

Compound	ΔE,[a] kcal/mol	$\Delta(\Delta H^0)$,[a] kcal/mol	$\Delta(\Delta G^0)$,[a] kcal/mol	d(M-NH_3), Å	N_α-M-N_α[b] angle, deg.
$ZnPcF_{16}\cdots NH_3$	-13.5	-11.9	-5.2	2.21	157
$CoPcF_{16}\cdots NH_3$	-10.4	-8.9	-1.5	2.29	173
$CuPcF_{16}\cdots NH_3$	-9.7[c]	-8.3[c]	-1.8[c]	2.46	173
$NiPcF_{16}\cdots NH_3$	-1.9	-1.3	4.1	3.37	179

[a] The $MPcF_{16}$+NH_3 asymptote is a reference for calculations of the relative thermodynamic properties. [b] The atomic labels are in accordance with Fig. 1. [c] Calculated at the B3LYP/6-311G(d,p) level of theory.

Figure captions

Figure 1. Chemical structure of $MPcF_{16}$.

Figure 2. Surface plasmon resonance curves for (a) pure gold-coated substrate; (b) gold/as-deposited $CuPcF_{16}$ film; and (c) gold/$CuPcF_{16}$ exposed by NH_3 gas (200 ppm).

Figure 3. Surface plasmon resonance (SPR) response curves of $MPcF_{16}$ thin films toward gaseous NH_3: (a) $NiPcF_{16}$, black; (b) $CuPcF_{16}$, red; (c) $CoPcF_{16}$, blue; (d) $ZnPcF_{16}$, green. The SPR response curves were recorded using the wavelength of λ=633 nm (He-Ne laser) at a fixed angle of incidence $\theta = 44.2^{o}$.

Figure 4. The experimental IR spectra of $MPcF_{16}$: (a) $NiPcF_{16}$, black; (b) $CuPcF_{16}$, red; (a) $CoPcF_{16}$, blue; (d) $ZnPcF_{16}$, green.

Figure 5. The experimental Raman spectra of $MPcF_{16}$: (a) $NiPcF_{16}$, black; (b) $CuPcF_{16}$, red; (a) $CoPcF_{16}$, blue; (d) $ZnPcF_{16}$, green.

Figure 6. Experimental (upper part) and calculated (lower part) IR spectra of $ZnPcF_{16}$ films before (a, black curves) and after (b, red curves) exposure to gaseous ammonia (200 ppm).

Figure 7. Refractive index change of the $MPcF_{16}$ films after exposure to ammonia vapor *vs* calculated relative electronic energies (ΔE) (a, blue); the shift of the position of the "inner ring breathing" IR band (at 955, 953, 947, 937 cm^{-1} for $NiPcF_{16}$, $CoPcF_{16}$, $CuPcF_{16}$ and $ZnPcF_{16}$, respectively) *vs* calculated relative electronic energies (b, red).

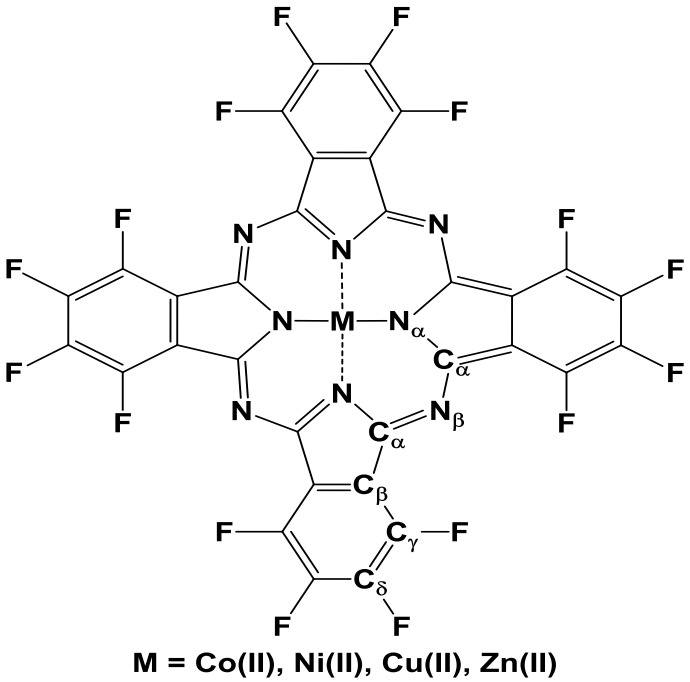

Figure 1. Chemical structure of $MPcF_{16}$.

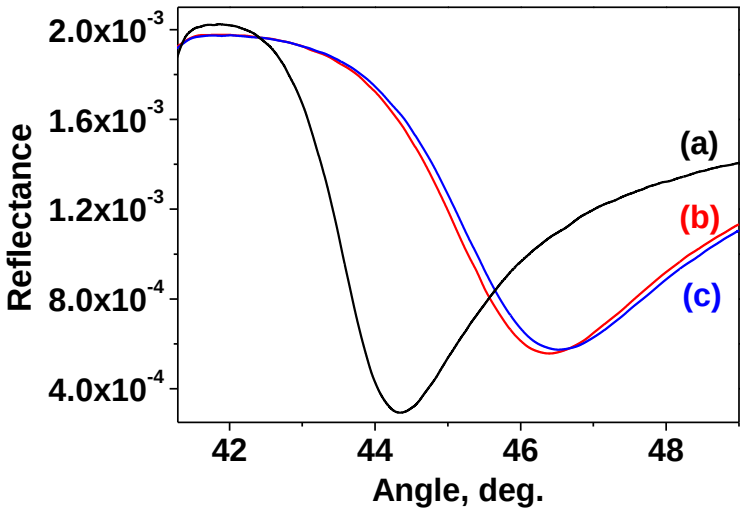

Figure 2. Surface plasmon resonance curves for (a) pure gold-coated substrate; (b) gold/as-deposited $CuPcF_{16}$ film; and (c) gold/$CuPcF_{16}$ exposed by NH_3 gas (200 ppm).

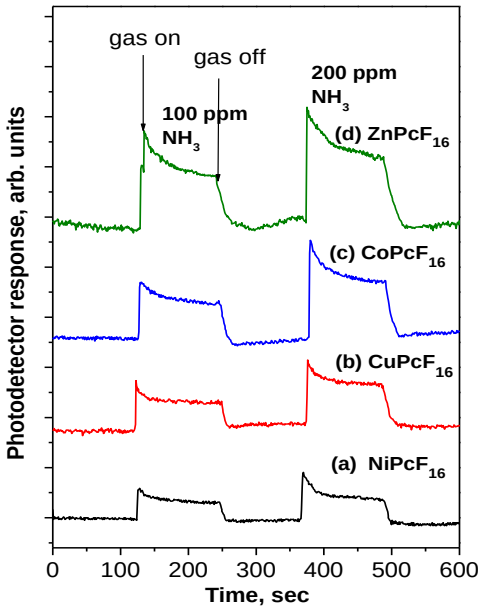

Figure 3. Surface plasmon resonance (SPR) response curves of $MPcF_{16}$ thin films toward gaseous NH_3 (100 ppm and 200 ppm, respectively): (a) $NiPcF_{16}$, black; (b) $CuPcF_{16}$, red; (c) $CoPcF_{16}$, blue; (d) $ZnPcF_{16}$, green. The SPR response curves were recorded using the wavelength of λ=633 nm (He-Ne laser) at a fixed angle of incidence $\theta = 44.2^{o}$.

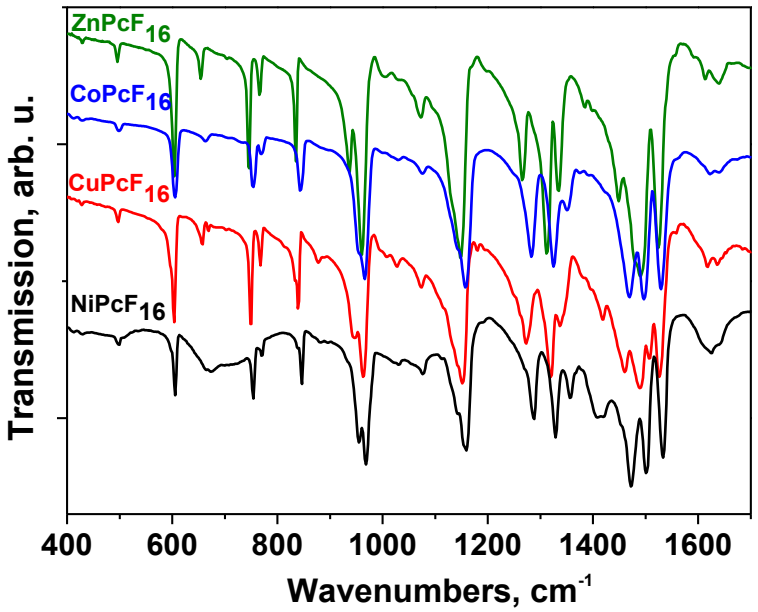

Figure 4. The experimental IR spectra of $MPcF_{16}$: (a) $NiPcF_{16}$, black; (b) $CuPcF_{16}$, red; (a) $CoPcF_{16}$, blue; (d) $ZnPcF_{16}$, green.

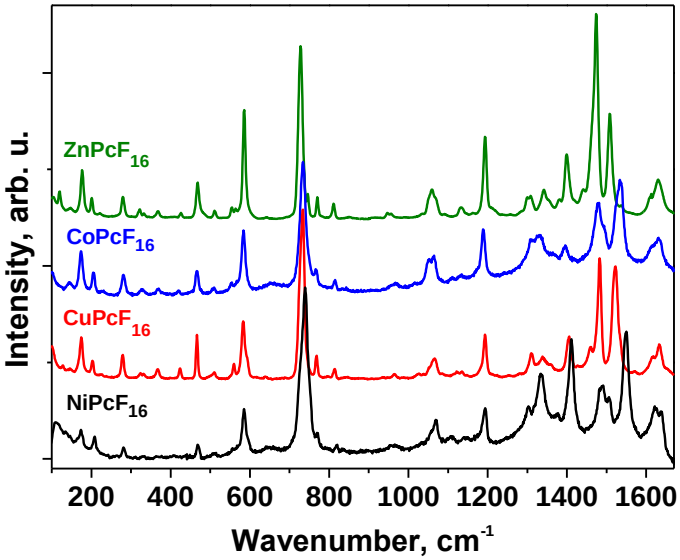

Figure 5. The experimental Raman spectra of $MPcF_{16}$: (a) $NiPcF_{16}$, black; (b) $CuPcF_{16}$, red; (a) $CoPcF_{16}$, blue; (d) $ZnPcF_{16}$, green.

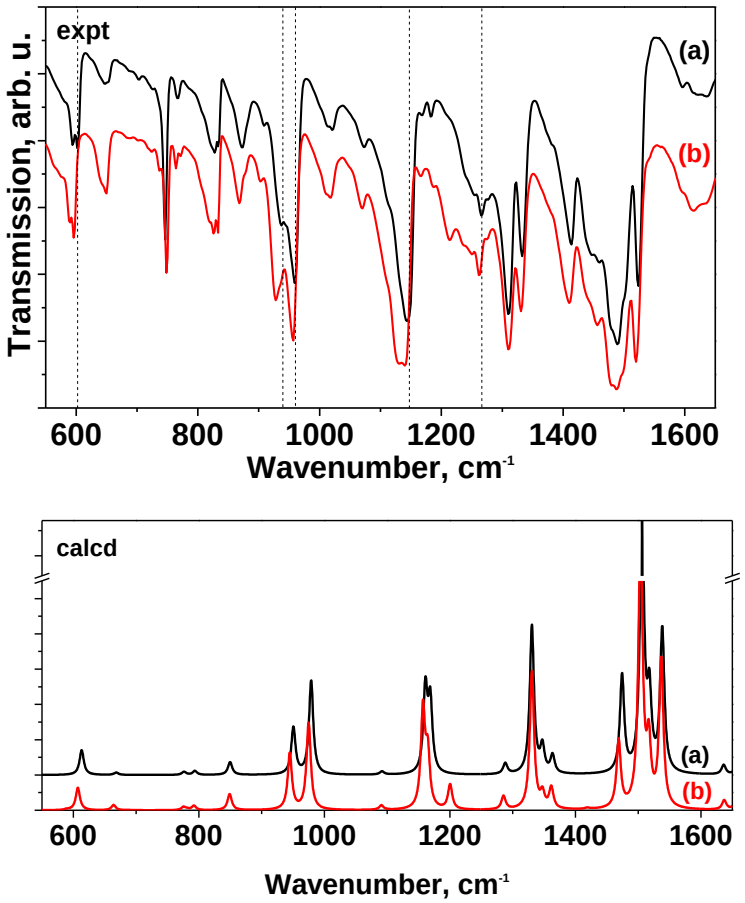

Figure 6. Experimental (upper part) and calculated (lower part) IR spectra of $ZnPcF_{16}$ films before (a, black curves) and after (b, red curves) exposure to gaseous ammonia (200 ppm).

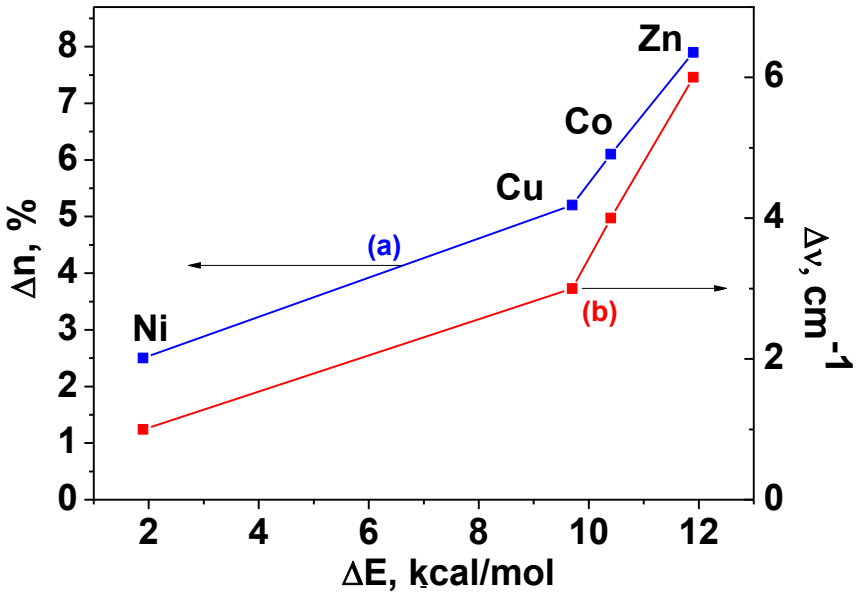

Figure 7. Refractive index change of the $MPcF_{16}$ films after exposure to ammonia vapor *vs* calculated relative electronic energies (ΔE) (a, blue); the shift of the position of the "inner ring breathing" IR band (at 955, 953, 947, 937 cm^{-1} for $NiPcF_{16}$, $CoPcF_{16}$, $CuPcF_{16}$ and $ZnPcF_{16}$, respectively) *vs* calculated relative electronic energies (b, red).